Supporting Information

In situ Coupling Reconstruction of Cobalt-Iron Oxide on Cobalt Phosphate Nanoarray with Interfacial Electronic Features for Highly Enhanced Water Oxidation Catalysis

Peng Guo, [†,//] *Zhaojie Wang,* [†,//,*] *Shaohui Ge,* [§] *Hongyu Chen,* [‡] *Jinbao Zhang,* [†] *Haowei Wang,* [†] *Siyuan Liu,* [†,*] *Shuxian Wei,* [‡] *Xiaoqing Lu* [†,*]

[†]School of Materials Science and Engineering, China University of Petroleum, 66 Changjiang West road, Huangdao District, Qingdao, Shandong 266580, P. R. China

[§]Petrochina Petrochemical Research Institute, No. 9, Chaoqian Road, Science and Technology Park, Changping District, Beijing 102206, P.R.China

[‡] College of Science, China University of Petroleum, 66 Changjiang West road, Huangdao District, Qingdao, Shandong 266580, P. R. China

[//] P.G. and Z.J.W. contributed equally to this work.

* E_mail: luxq@upc.edu.cn

*E_mail: wangzhaojie@upc.edu.cn

*E_mail: lsy@upc.edu.cn

Number of pages: 30

Number of figures: 22

Number of tables: 3

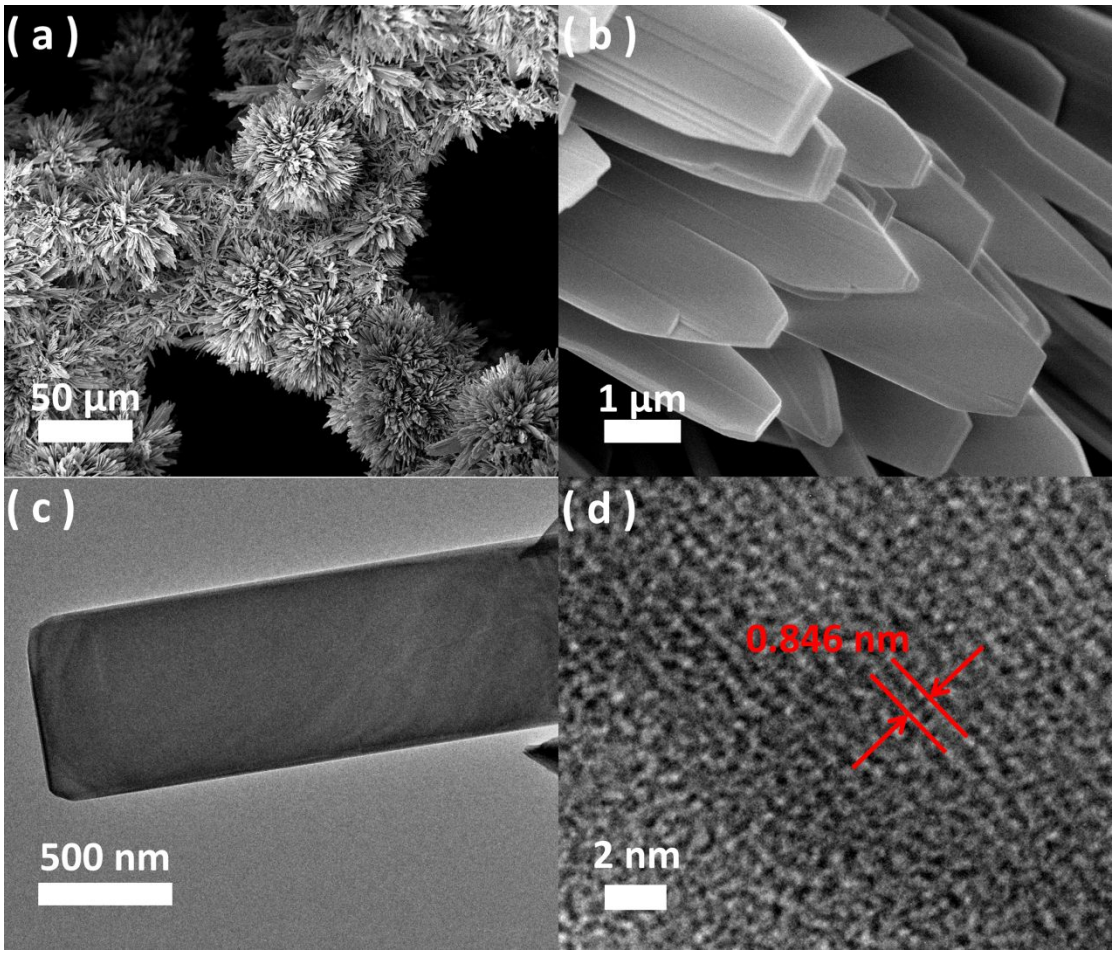

Figure S1. The morphology characterization of CoPi@NF. SEM images of CoPi@NF with (a) low and (b) high magnifications. (c) TEM image of CoPi@NF. (d) HRTEM image of CoPi@NF.

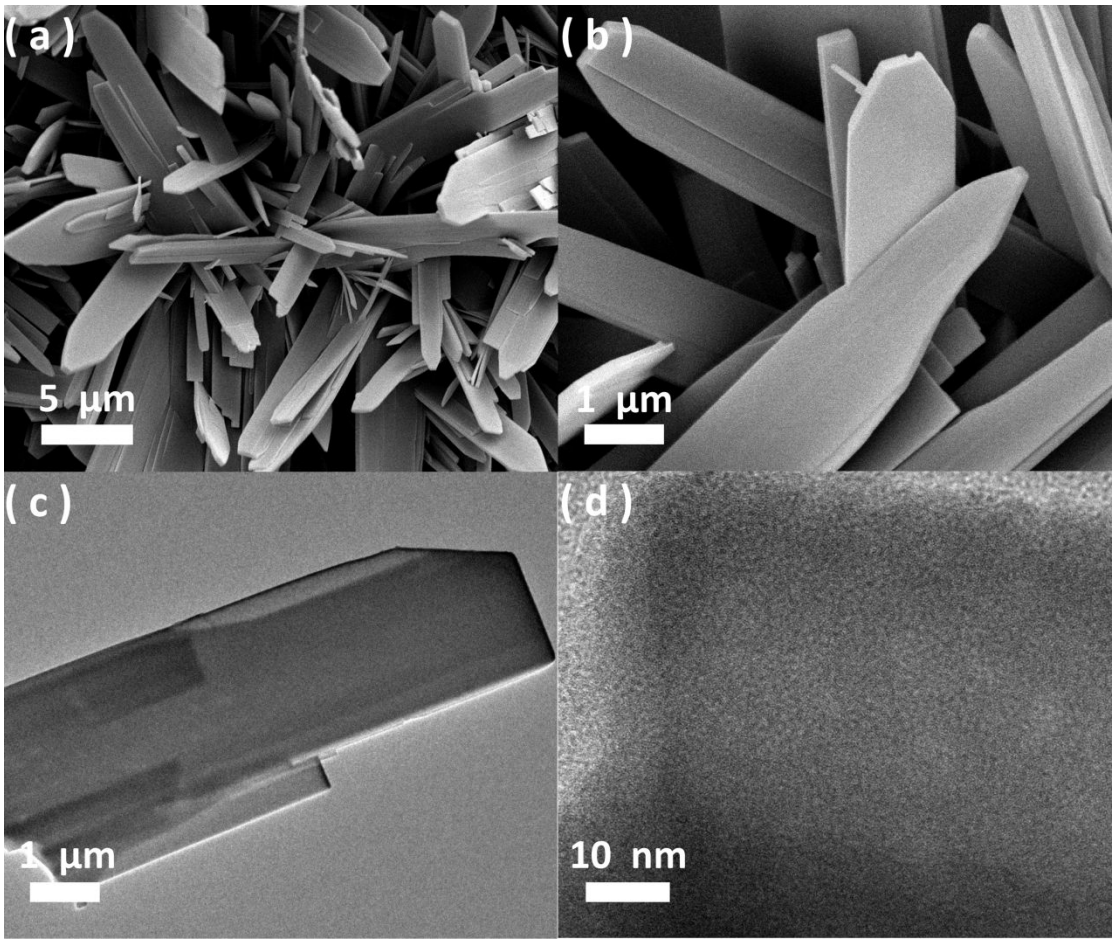

Figure S2. (a) and (b) SEM images of CoPi-350@NF with different magnifications.

(c) TEM image and (d) HRTEM image of the CoPi-350@NF.

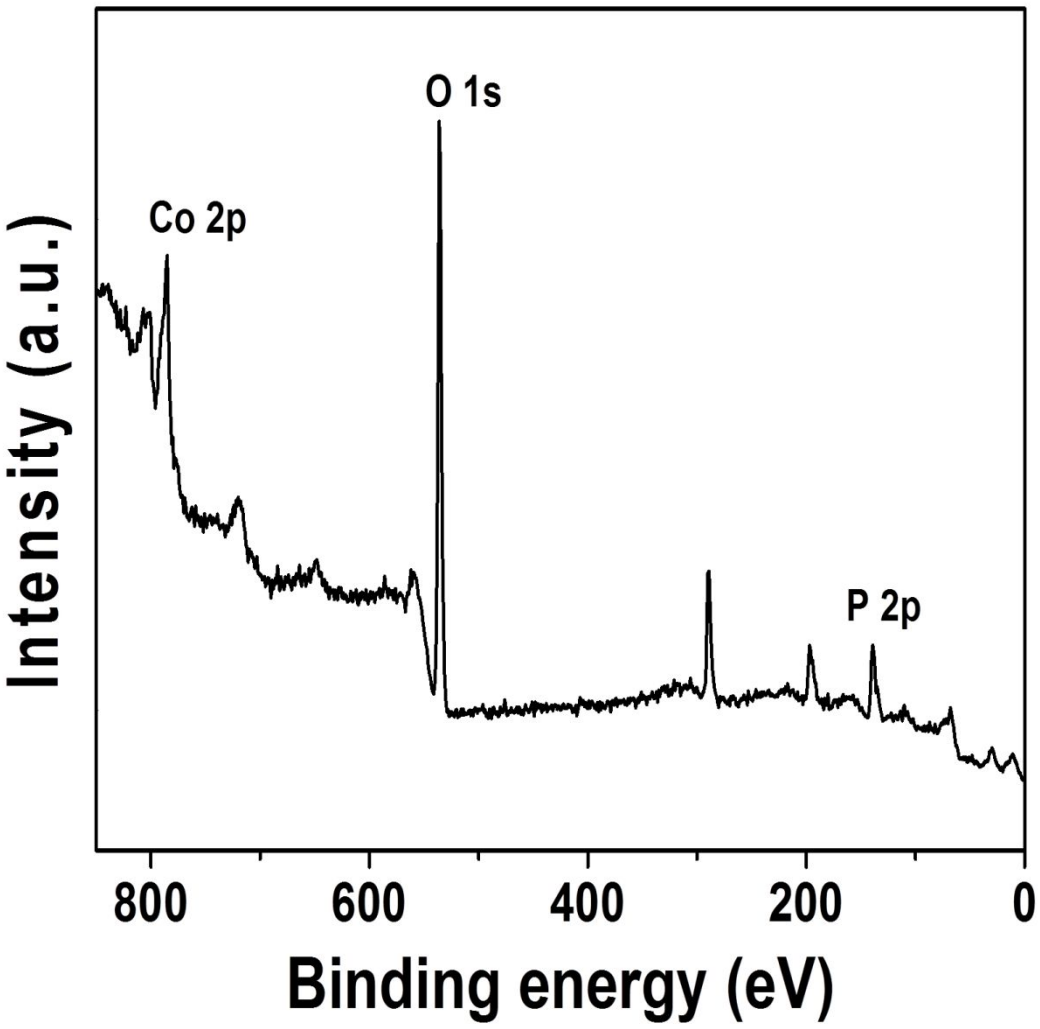

Figure S3. The XPS survey spectrum of CoPi-350@NF.

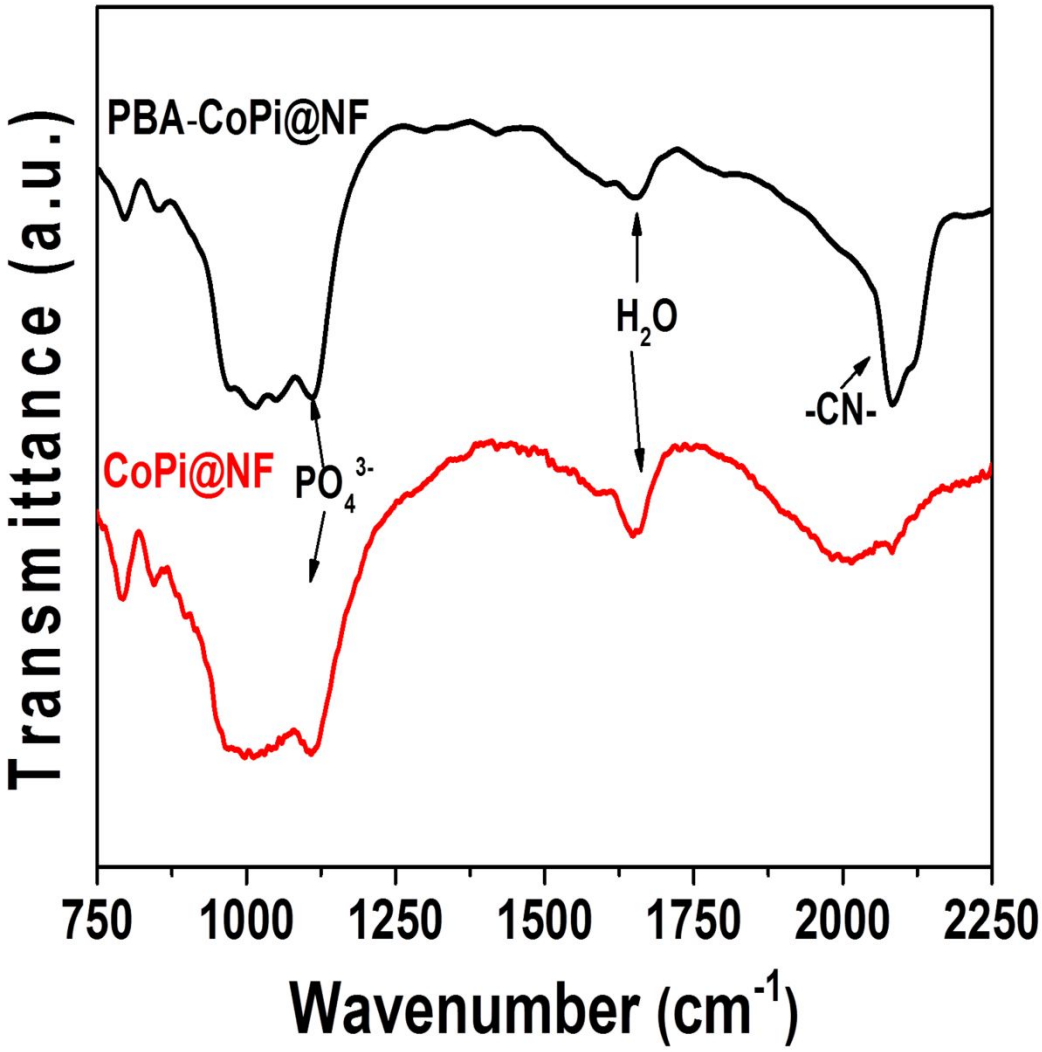

Figure S4. FTIR spectra of CoPi@NF and the PBA-CoPi@NF.

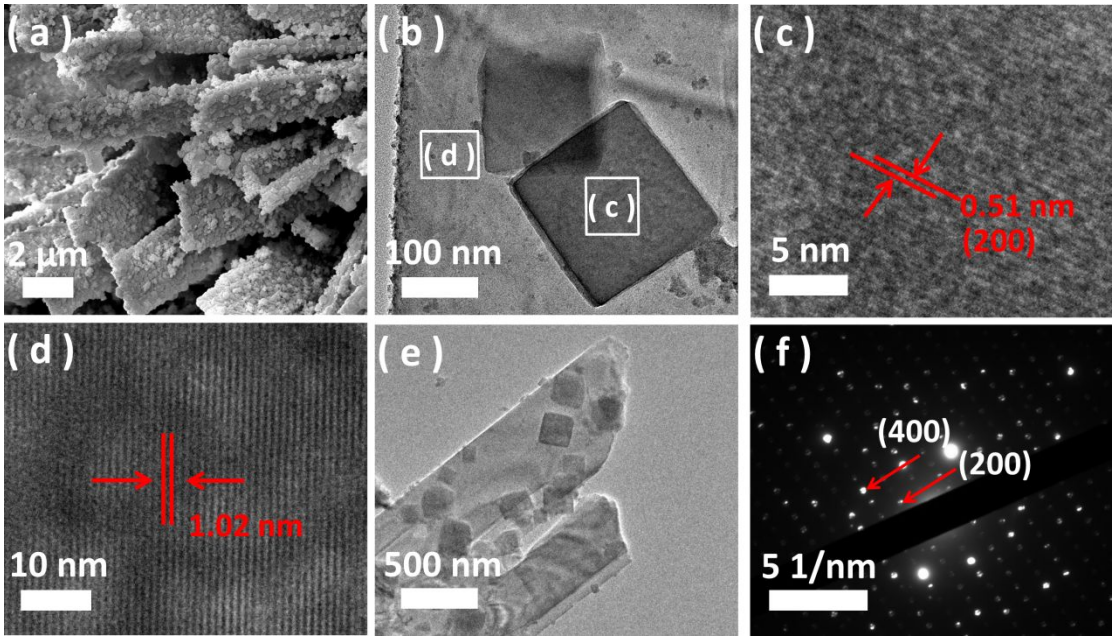

Figure S5. (a) SEM image of PBA-CoPi@NF. (b) TEM image of the PBA-CoPi@NF with PBA nanocubes decorated on CoPi. (c) and (d) The corresponding HRTEM images of the PBA-CoPi@NF as shown in (b). (e) TEM image and (f) corresponding SAED image of PBA-CoPi@NF.

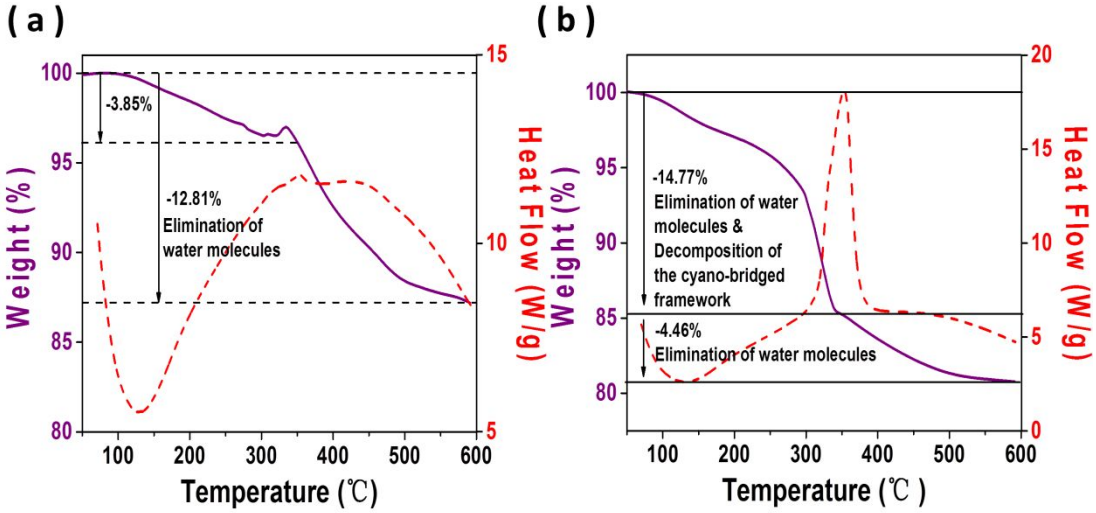

Figure S6. TGA and DSC plots of (a) CoPi@NF and (b) PBA-CoPi@NF.

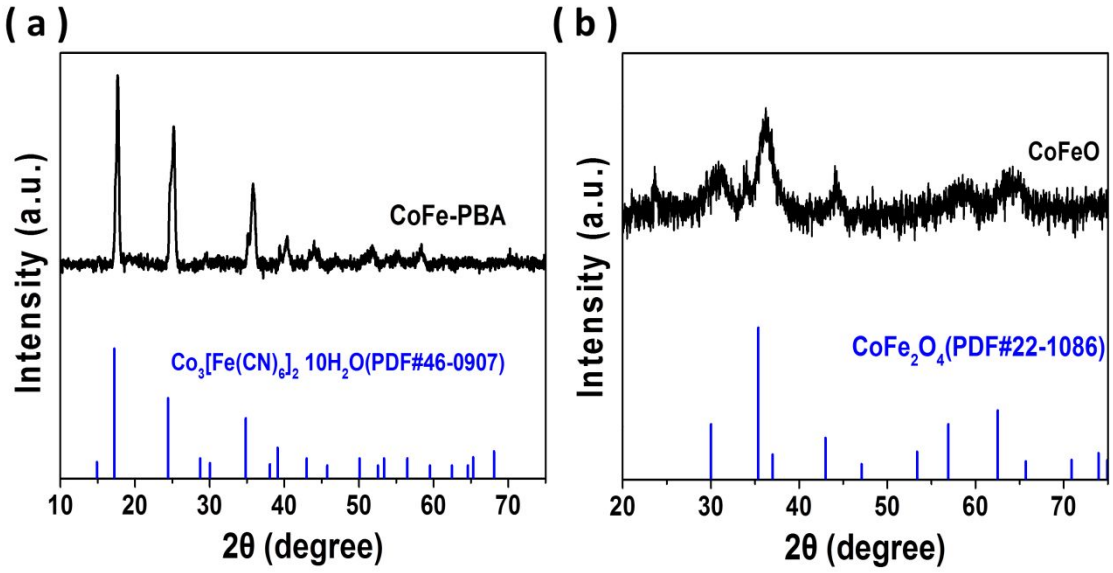

Figure S7. XRD patterns of (a) CoFe-PBA and (b) CoFeO.

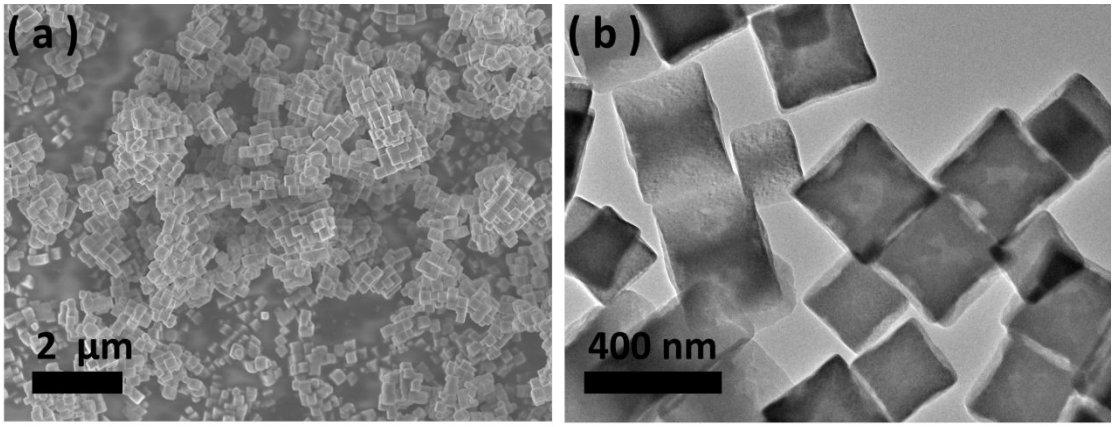

Figure S8. The (a) SEM and (b) TEM images of CoFe-PBA.

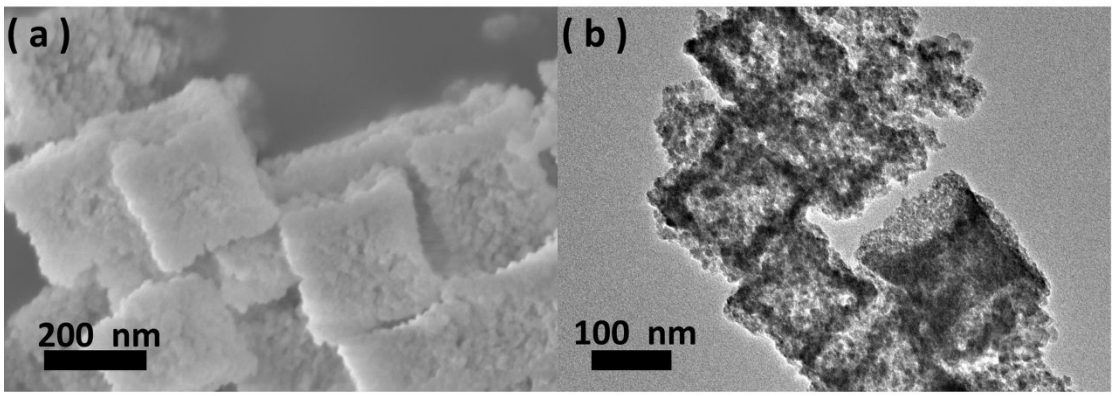

Figure S9. The (a) SEM and (b) TEM images of CoFeO.

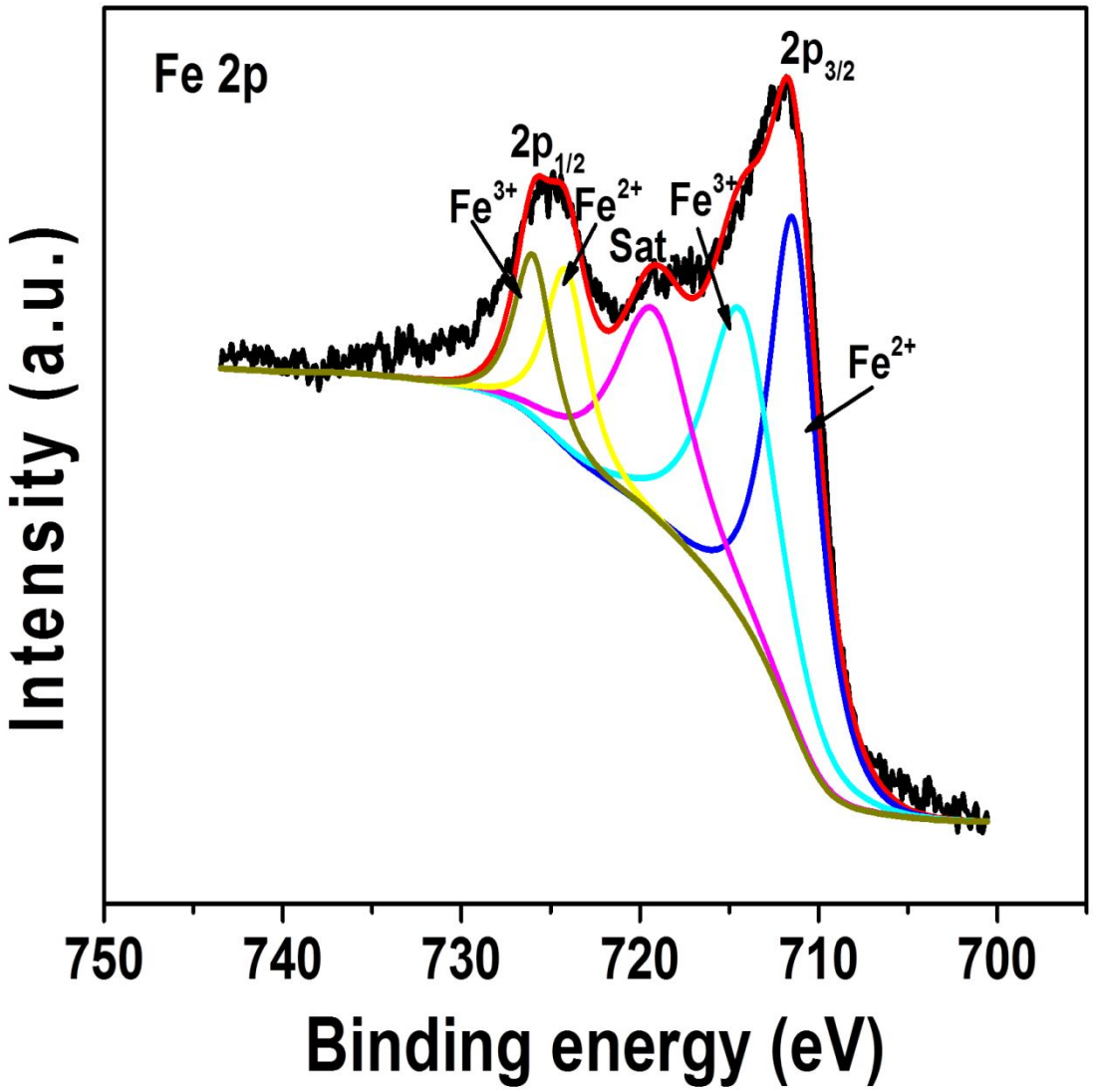

Figure S10. High resolution XPS Fe spectra of CoFeO-CoPi@NF.

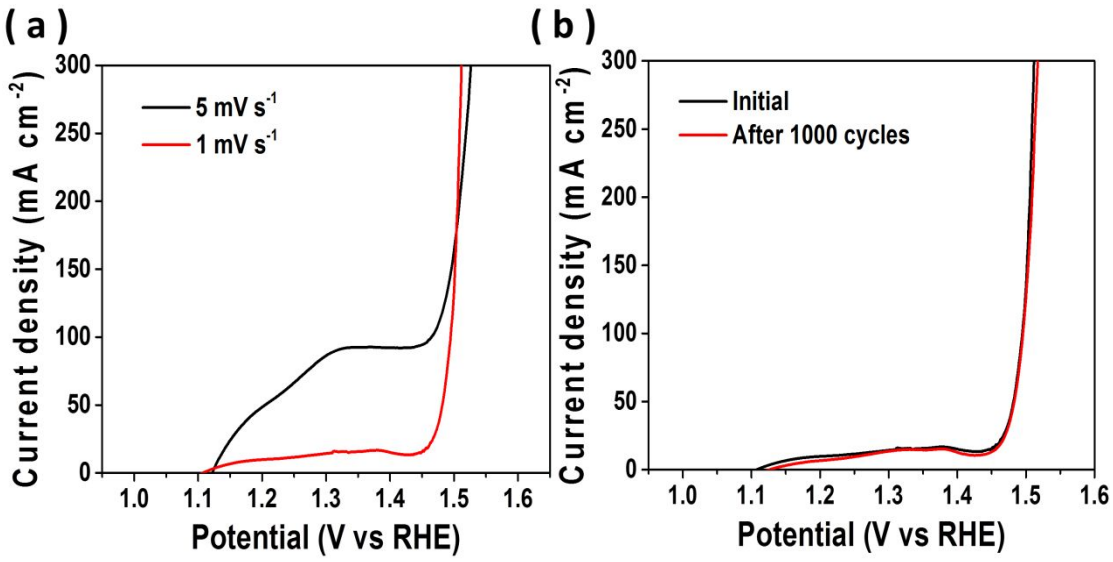

Figure S11. (a) LSV curves of CoFeO-CoPi@NF at different scan rates. (b) LSV curves before and after OER test at a scan rate of 1 mV s^{-1}.

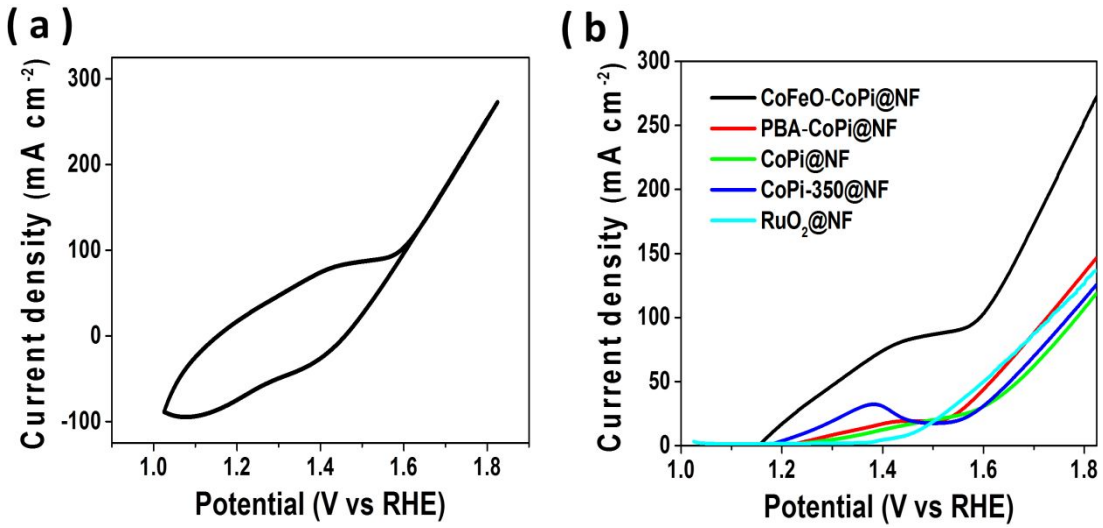

Figure S12. (a) CV curves of the CoFeO-CoPi@NF and (b) LSV curves without iR compensation of the as-prepared materials and commercial RuO_2@NF.

The cathodic sweep CV curves were recorded to measure the onset overpotential of the CoFeO-CoPi@NF according to recent reports.[S1] When the current density current density is zero, the potential is 1.45 V, as a result, the onset overpotential of CoFeO-CoPi@NF is 220 mV.

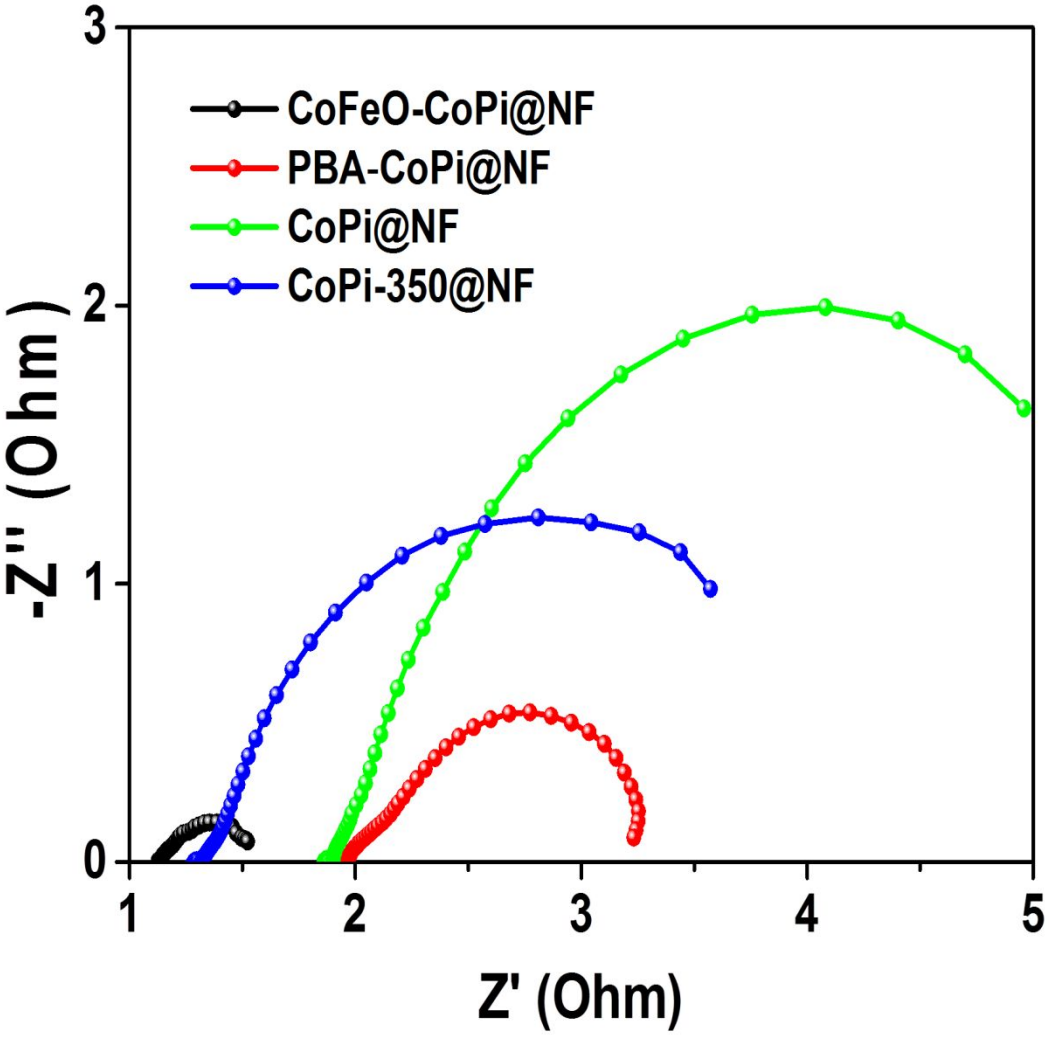

Figure S13. EIS Nyquist plots of the as-prepared materials.

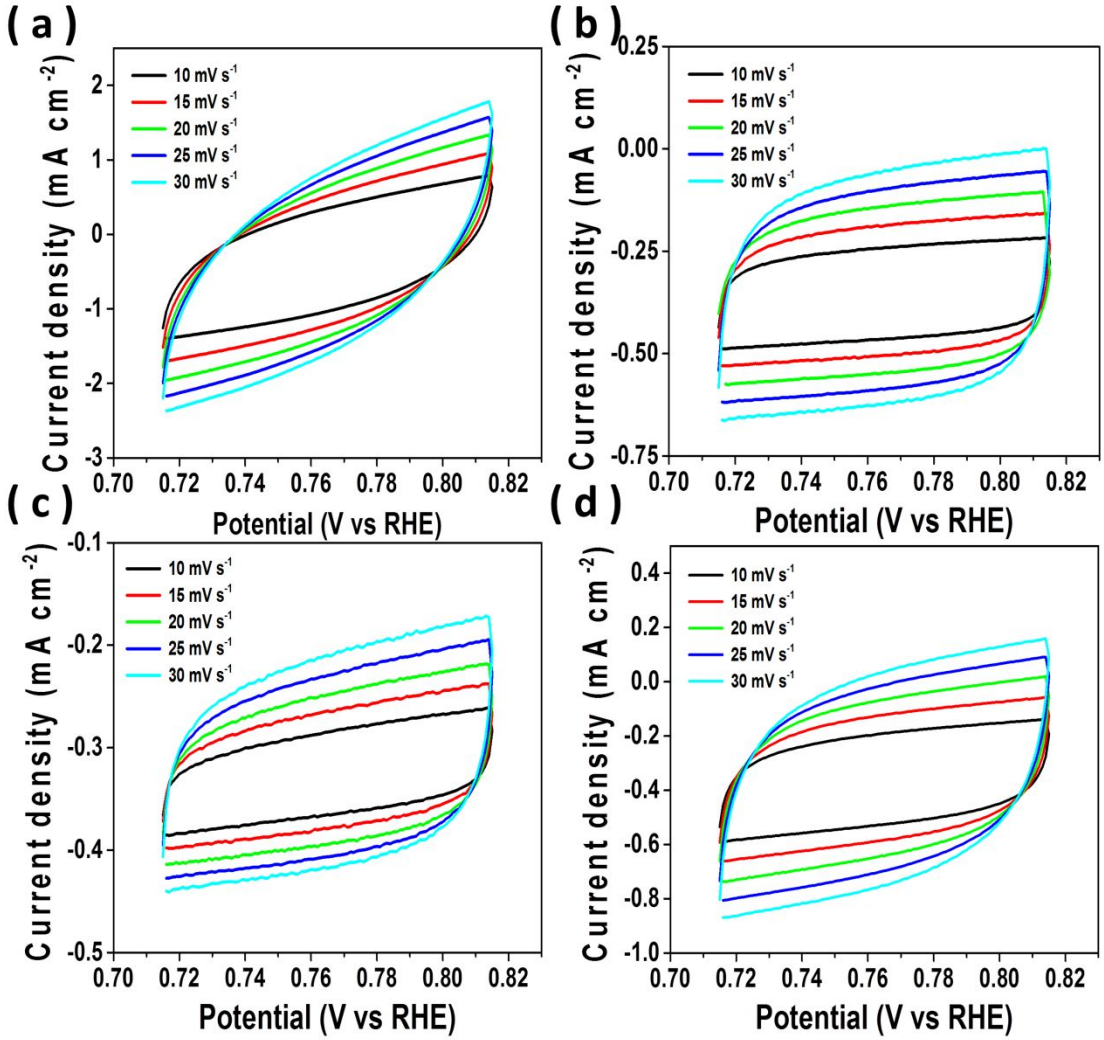

Figure S14. CV curves of (a) CoFeO-CoPi@NF, (b) PBA-CoPi@NF, (c) CoPi@NF and (d) CoPi-350@NF at different scan rates in a potential window from 0.715 V to 0.815 V vs RHE.

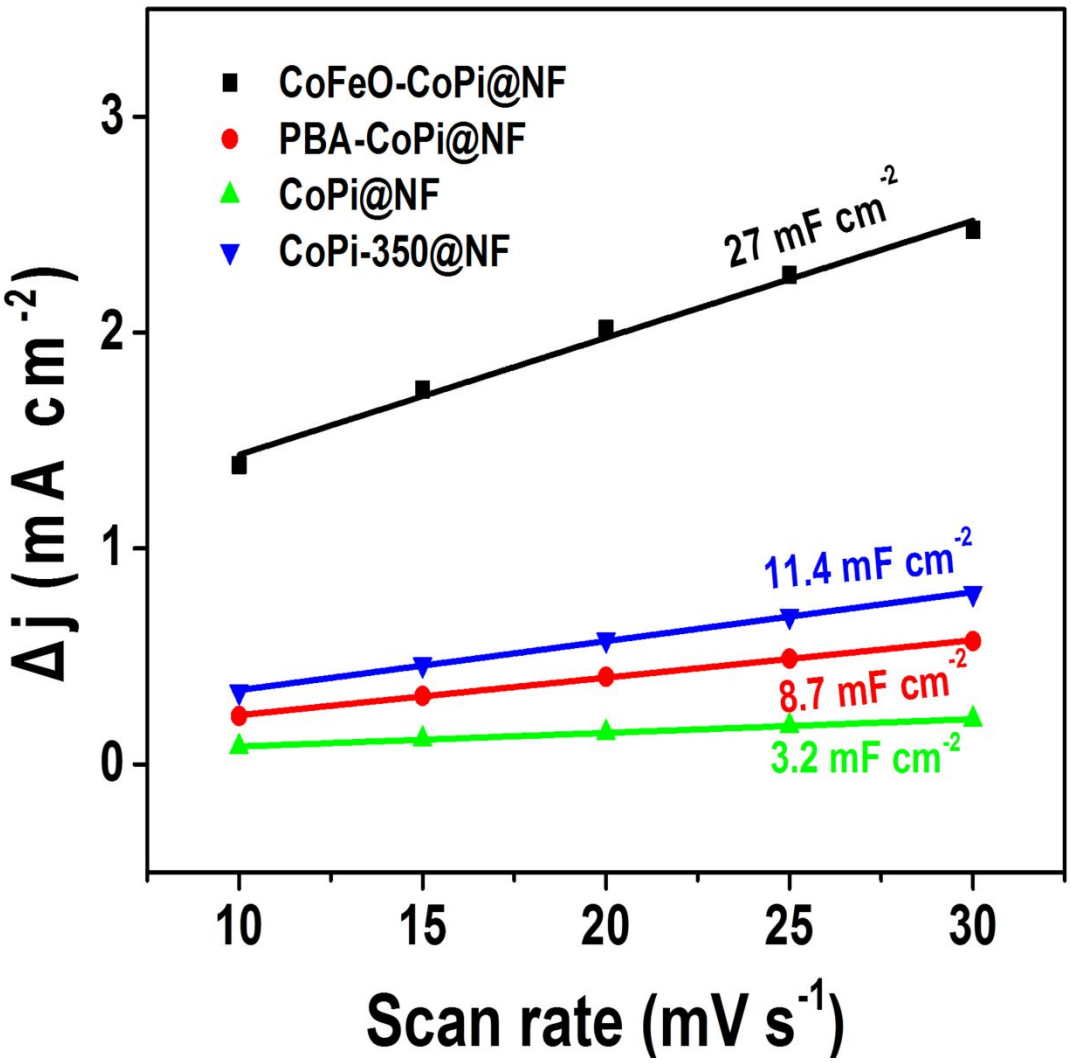

Figure S15. Capacitive current density against scan rate.

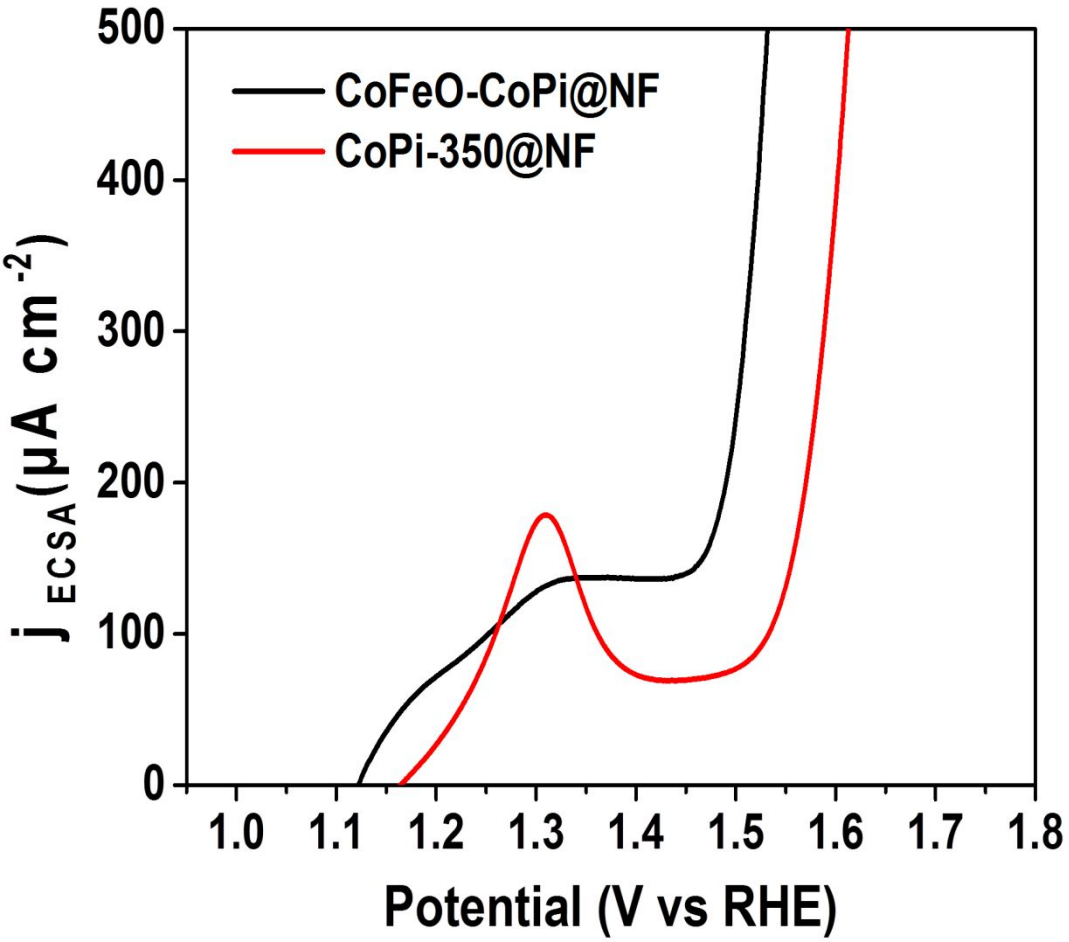

Figure S16. The OER Polarization curves of CoFeO-CoPi@NF and CoPi-350@NF with normalization by ECSA. The ECSA of CoFeO-CoPi@NF and CoPi-350@NF are shown in Table S1.

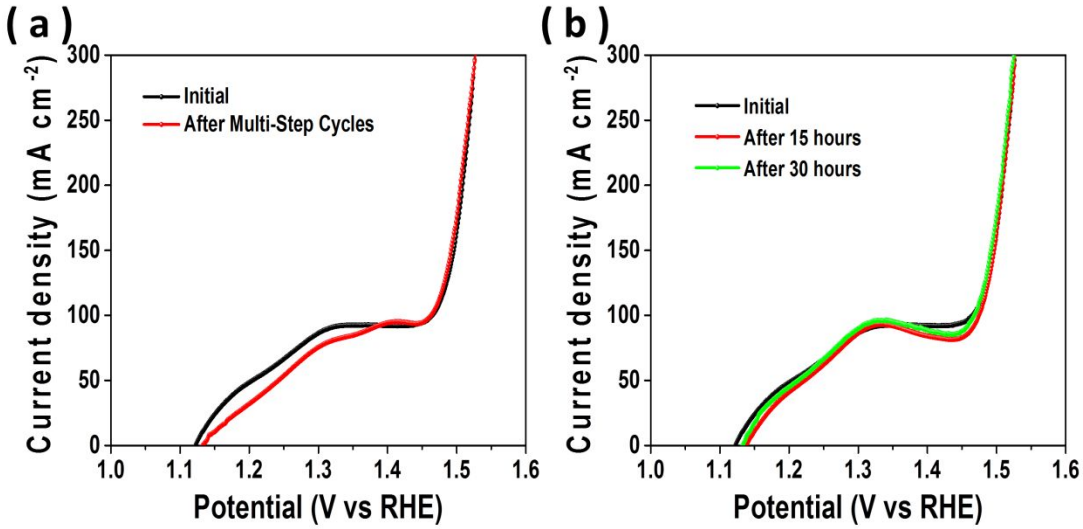

Figure S17. (a) LSV curves of the CoFeO-CoPi@NF before and after multiple current densities cycles. (b) LSV curves of the CoFeO-CoPi@NF before and after chronopotentiometric test.

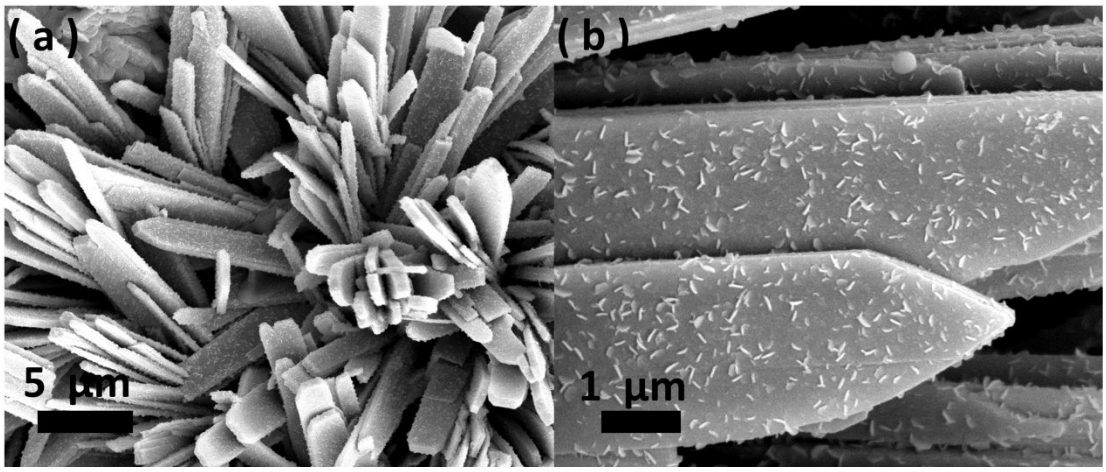

Figure S18. (a) Low resolution and (b) high resolution SEM images of the CoPi-350@NF after OER test.

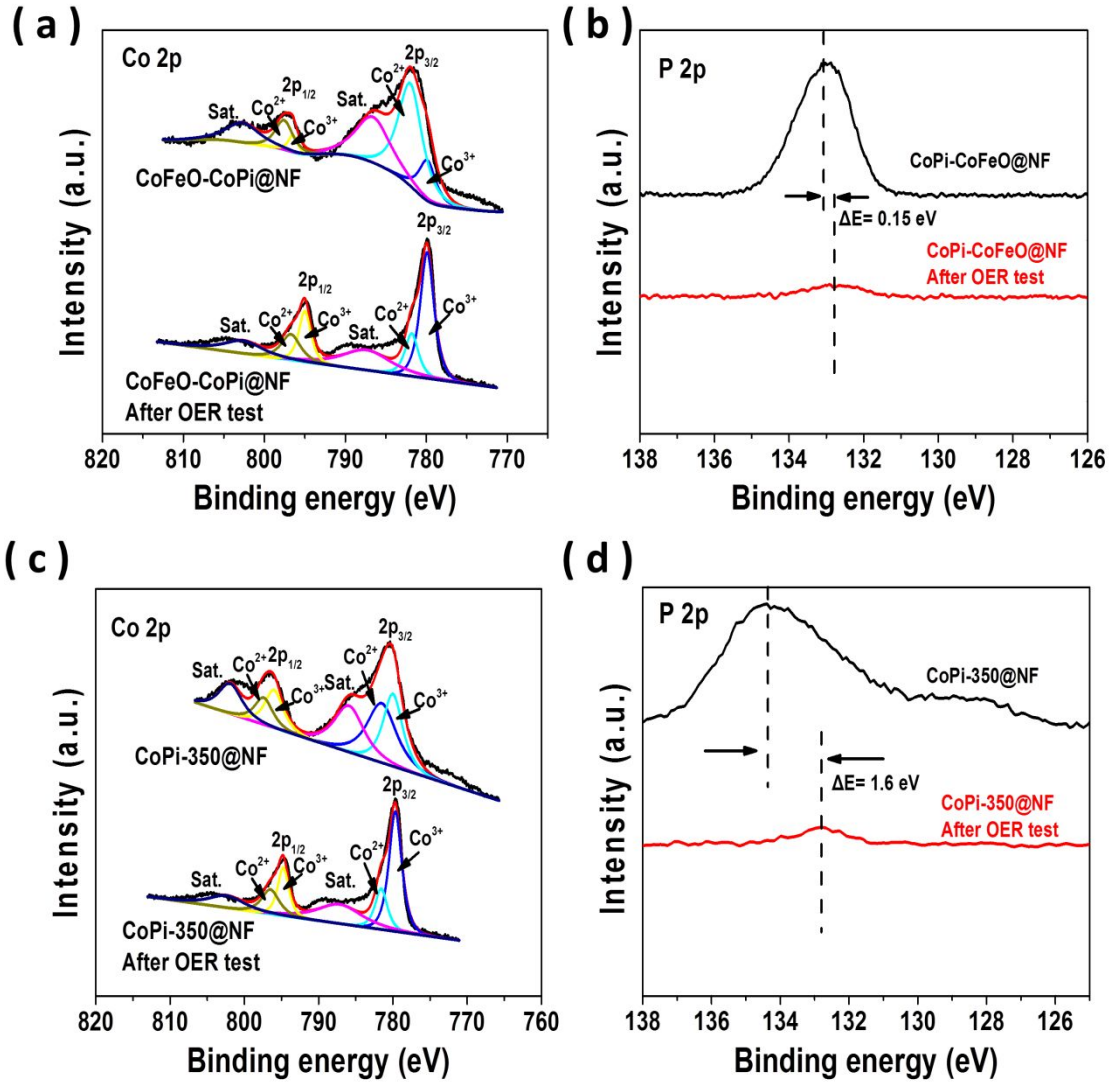

Figure S19. High resolution XPS (a) Co 2p and (b) P 2p spectra of CoFeO-CoPi@NF before and after OER test. XPS (c) Co 2p and (d) P 2p spectra of CoPi-350@NF before and after OER test.

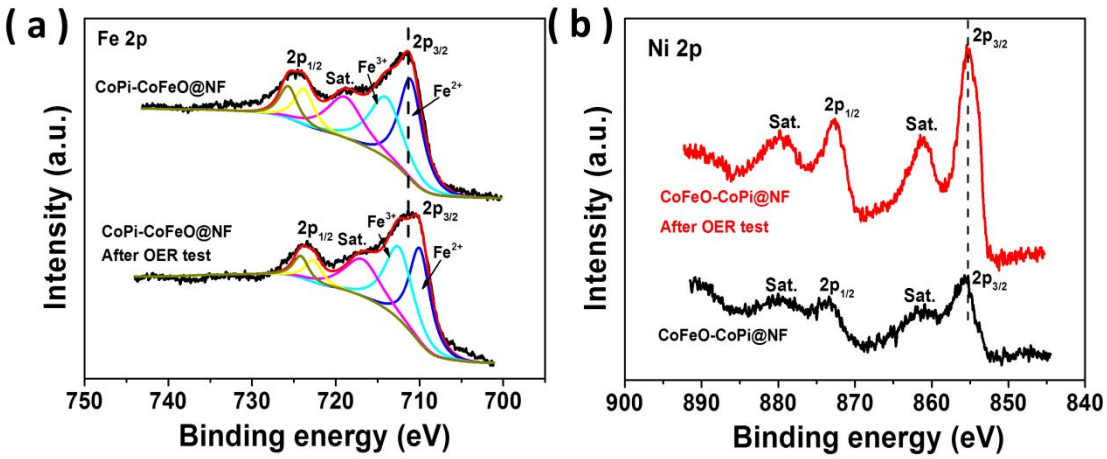

Figure S20. High resolution XPS (a) Fe 2p and (b) Ni 2p spectra before and after OER test.

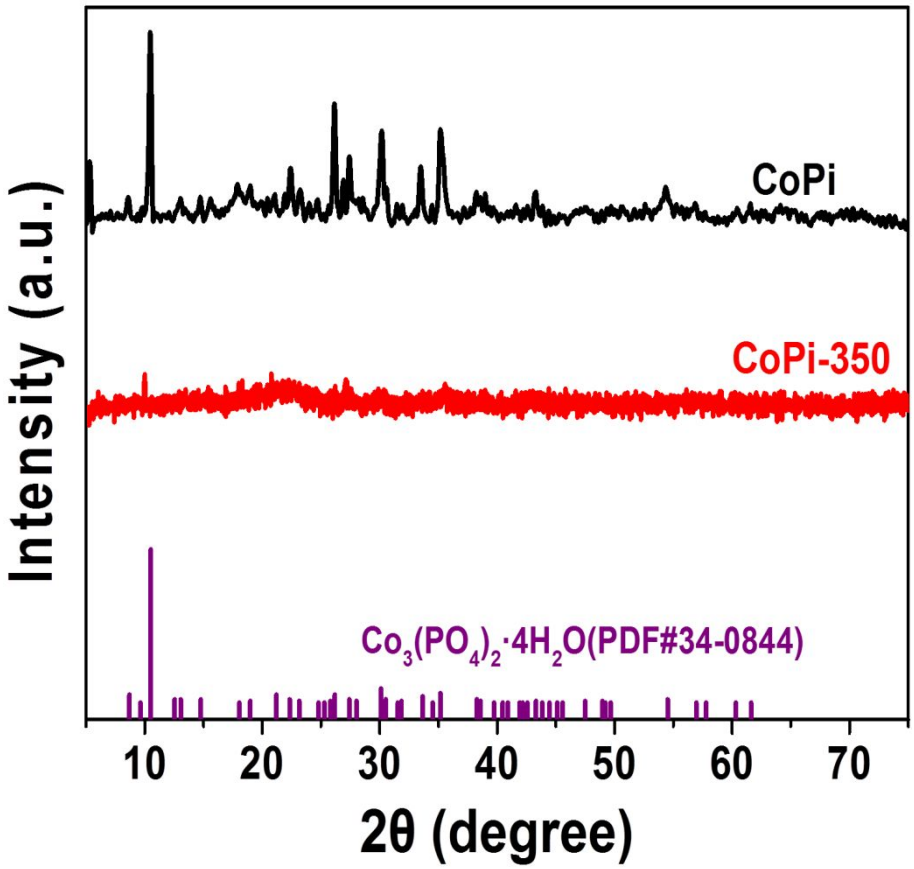

Figure S21. XRD pattern of CoPi and CoPi-350.

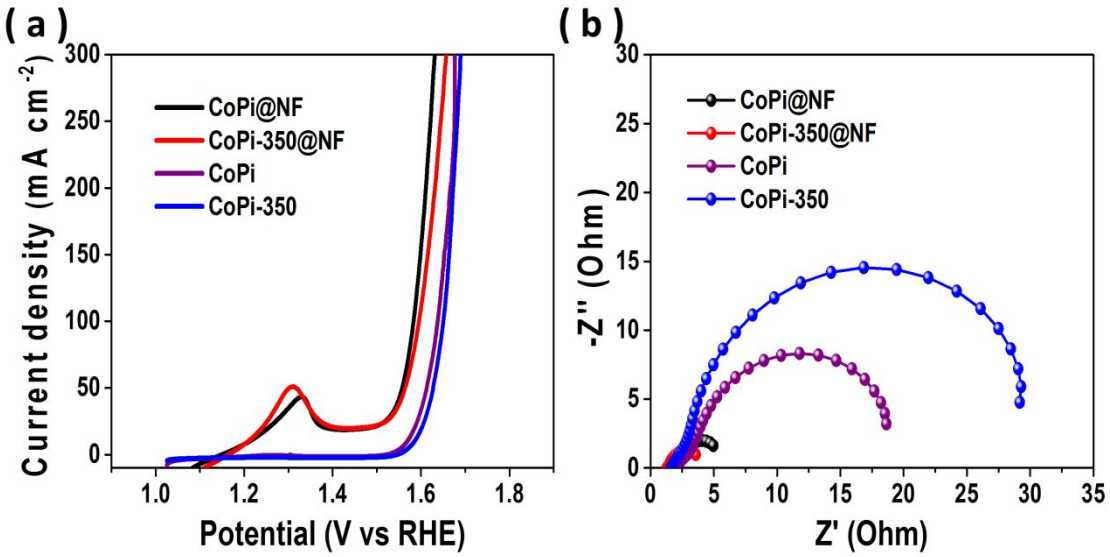

Figure S22. (a) LSV curves of catalysts, (b) EIS Nyquist plots of catalysts.

Firstly, according to the LSV curves shown in the Figure 4a, the CoFeO-CoPi@NF attain a current density of 300 mA cm^{-2} at an overpotential of 292 mV while the onset overpotential of Ni foam is 330 mV, which suggests the main active sites were on the CoFeO-CoPi@NF. In addition, no obviously change of Ni 2p spectra before and after OER test of CoFeO-CoPi@NF was detected shown as shown in Figure S20b further demonstrate the main active site is cobalt. To get a better understanding of the role of Ni foam in OER, we prepared the CoPi and CoPi-350 powder in the same method, the XRD of CoPi and CoPi-350 shown in Figure S18 suggests the same crystal structure as the CoPi@NF and CoPi-350@NF. And then we coat the CoPi and CoPi-350 powder on the carbon paper to study the role of Ni foam in OER. The LSV curves shown in Figure S22a indicate a better OER performance of CoPi@NF and CoPi-350@NF. Moreover, the EIS Nyquist plots shown in Figure S22b suggest that the CoPi@NF and CoPi-350@NF exhibit better conductivity. As a result, the Ni foam could improve the conductivity to enhance the OER performance.

Table S1 The C_{dl} and normalized ECSA of CoFeO-CoPi@NF and CoPi-350@NF.

Sample	**CoFeO-CoPi@NF**	**CoPi-350@NF**
C_{dl}	27 mF cm^{-2}	11.4 mF cm^{-2}
ECSA	675 cm^2	285 cm^2

Table S2 Recent progress of the electrocatalysts for the oxygen evolution.

Catalysis	Electrolyte	Overpotential	Tafel slope	Ref
CoFeO-CoPi@ NF	**1 M KOH**	**235 mV (100mA cm^{-2})**	**56 mV dec^{-1}**	**This work**
Co@N-CS/N-HCP@CC	1 M KOH	248 mV (10 mA cm^{-2})	68 mV dec^{-1}	S2
NiCoFeP	1 M KOH	273 mV (10 mA cm^{-2})	56 mV dec^{-1}	S3
Fe_1Co_1-ONS	0.1 M KOH	308 mV (10 mA cm^{-2})	36.8 mV dec^{-1}	S4
Co_9S_8 −NSC@M_2C	1 M KOH	293 mV (10 mA cm^{-2})	59.7 mV dec^{-1}	S5
$(Ni_2Co_1)_{0.925}$ Fe $_{0.075}$ -MOF-NF	1 M KOH	257 mV (10 mA cm^{-2})	41.3 mV dec^{-1}	S6
NiCoFe LTHs/CFC	1 M KOH	239 mV (10 mA cm^{-2})	32 mV dec^{-1}	S7
CoFePi	0.1 M KOH	315 (10 mA cm^{-2})	33 mV dec^{-1}	S8
nPBA@$Co(OH)_2$ /NF	1 M KOH	290 (20 mA cm^{-2})	46 mV dec^{-1}	S9
$Co_{1.8}Ni(OH)_{5.6}$ @$Co_{1.8}NiS_{0.4}$ $(OH)_{4.8}$	0.1 M KOH	274 (10 mA cm^{-2})	45 mV dec^{-1}	S10
FeS_2/CoS_2 NSs	1 M KOH	302 mV (100 mA cm^{-2})	42 mV dec^{-1}	S11
Co_3O_4/Co-Fe oxide	1 M KOH	297 mV (10 mA cm^{-2})	61 mV dec^{-1}	S12
$A_{2.7}$B-MOF-FeC $o_{1.6}$	1 M KOH	288 mV (10 mA cm^{-2})	39 mV dec^{-1}	S13

$NiFe^{II}$-PBA	1 M KOH	285 mV ($50\ mA\ cm^{-2}$)	53.1 mV dec^{-1}	S14
Co_3O_4@C-N NSA/NiF	1 M KOH	245 mV ($20\ mA\ cm^{-2}$)	63 mV dec^{-1}	S15
CoFeZr oxides	1 M KOH	248 mV ($10\ mA\ cm^{-2}$)	54.2 mV dec^{-1}	S16

Table S3. Comparison of the P atomic contents in CoFeO-CoPi@NF and CoPi-350@NF before and after OER test.

Atomic content	Initial	After OER test
CoFeO-CoPi@NF	12.89	2.27
CoPi-350@NF	27.12	2.67

References

(S1) Duan, J.; Chen, S.; Zhao, C. Ultrathin metal-organic framework array for efficient electrocatalytic water splitting. *Nat. Commun.* **2017**, 8, 15341.

(S2) Chen, Z.; Ha, Y.; Jia, H.; Yan, X.; Chen, M.; Liu, M.; Wu, R. Oriented Transformation of Co‐LDH into 2D/3D ZIF‐67 to Achieve Co‐N‐C Hybrids for Efficient Overall Water Splitting. *Adv. Energy Mater.* **2019**, 1803918.

(S3) Guo, Y.; Tang, J.; Wang, Z.; Sugahara, Y.; Yamauchi, Y. Hollow Porous Heterometallic Phosphide Nanocubes for Enhanced Electrochemical Water Splitting. *Small* **2018**, 14, 1802442.

(S4) Zhuang, L.; Ge, L.; Yang, Y.; Li, M.; Jia, Y.; Yao, X.; Zhu, Z. Ultrathin Iron‐Cobalt Oxide Nanosheets with Abundant Oxygen Vacancies for the Oxygen Evolution Reaction. *Adv. Mater.* **2017**, 29, 1606793.

(S5) Luo, X.; Zhou, Q.; Du, S.; Li, J.; Zhong, J.; Deng, X.; Liu, Y. Porous Co9S8/Nitrogen, Sulfur-Doped Carbon@Mo_2C Dual Catalyst for Efficient Water Splitting. *ACS Appl. Mater. Interfaces* **2018**, 10, 22291-22302.

(S6) Qian, Q.; Li, Y.; Liu, Y.; Yu, L.; Zhang, G. Ambient Fast Synthesis and Active Sites Deciphering of Hierarchical Foam‐Like Trimetal‐Organic Framework Nanostructures as a Platform for Highly Efficient Oxygen Evolution Electrocatalysis. *Adv. Mater.* **2019**, 1901139.

(S7) Wang, A.-L.; Xu, H.; Li, G.-R. NiCoFe layered triple hydroxides with porous structures as high-performance electrocatalysts for overall water splitting. *ACS Energy Lett.* **2016**, 1, 445-453.

(S8) Zhou, Y.; Zeng, H. C. 3D networks of CoFePi with hierarchical porosity for effective OER electrocatalysis. *Small* **2018**, 14, 1704403.

(S9) Wang, Y.; Ma, J.; Wang, J.; Chen, S.; Wang, H.; Zhang, J. Interfacial Scaffolding Preparation of Hierarchical PBA‐Based Derivative Electrocatalysts for Efficient Water Splitting. *Adv. Energy Mater.* **2019**, 9, 1802939.

(S10) Wang, B.; Tang, C.; Wang, H. F.; Chen, X.; Cao, R.; Zhang, Q. A Nanosized CoNi Hydroxide@ Hydroxysulfide Core–Shell Heterostructure for Enhanced Oxygen Evolution. *Adv. Mater*. **2019**, 31, 1805658.

(S11) Li, Y.; Yin, J.; An, L.; Lu, M.; Sun, K.; Zhao, Y. Q.; Gao, D.; Cheng, F.; Xi, P. FeS_2/CoS_2 Interface nanosheets as efficient bifunctional electrocatalyst for overall water splitting. *Small* **2018**, 14, 1801070.

(S12) Wang, X.; Yu, L.; Guan, B. Y.; Song, S.; Lou, X. W. Metal‐Organic Framework Hybrid‐Assisted Formation of Co_3O_4/Co‐Fe Oxide Double‐Shelled Nanoboxes for Enhanced Oxygen Evolution. *Adv. Mater.* **2018**, 30, 1801211.

(S13) Xue, Z.; Li, Y.; Zhang, Y.; Geng, W.; Jia, B.; Tang, J.; Bao, S.; Wang, H. P.; Fan, Y.; Wei, Z. w. Modulating Electronic Structure of Metal‐Organic Framework for Efficient Electrocatalytic Oxygen Evolution. *Adv. Energy Mater.* **2018**, 8, 1801564.

(S14) Zeng, Y.; Chen, G.-F.; Jiang, Z.; Ding, L.-X.; Wang, S.; Wang, H. Confined heat treatment of a Prussian blue analogue for enhanced electrocatalytic oxygen evolution. *J. Mater. Chem. A* **2018**, 6, 15942-15946.

(S15) Kuang, X.; Luo, Y.; Kuang, R.; Wang, Z.; Sun, X.; Zhang, Y.; Wei, Q. Metal

organic framework nanofibers derived Co_3O_4-doped carbon-nitrogen nanosheet arrays for high efficiency electrocatalytic oxygen evolution. *Carbon* **2018**, 137, 433-441.

(S16) Huang, L.; Chen, D.; Luo, G.; Lu, Y. R.; Chen, C.; Zou, Y.; Dong, C. L.; Li, Y.; Wang, S. Zirconium‐Regulation‐Induced Bifunctionality in 3D Cobalt‐Iron Oxide Nanosheets for Overall Water Splitting. *Adv. Mater.* **2019**, 1901439.